NASA TECHNICAL NOTE

NASA TN D-3284

EFFECT OF NACELLE ORIENTATION ON THE AERODYNAMIC CHARACTERISTICS OF AN ARROW WING-BODY CONFIGURATION AT MACH NUMBER 2.03

by Emma Jean Landrum

Langley Research Center
Langley Station, Hampton, Va.

NATIONAL AERONAUTICS AND SPACE ADMINISTRATION • WASHINGTON, D. C. • FEBRUARY 1966

EFFECT OF NACELLE ORIENTATION ON THE AERODYNAMIC CHARACTERISTICS OF AN ARROW WING-BODY CONFIGURATION AT MACH NUMBER 2.03

By Emma Jean Landrum

Langley Research Center
Langley Station, Hampton, Va.

NATIONAL AERONAUTICS AND SPACE ADMINISTRATION

For sale by the Clearinghouse for Federal Scientific and Technical Information
Springfield, Virginia 22151 – Price $1.00

EFFECT OF NACELLE ORIENTATION ON THE AERODYNAMIC CHARACTERISTICS OF AN ARROW WING-BODY CONFIGURATION AT MACH NUMBER 2.03

By Emma Jean Landrum
Langley Research Center

SUMMARY

The investigation was performed in the Langley 4- by 4-foot supersonic pressure tunnel at a Reynolds number based on the wing mean aerodynamic chord of 4.05×10^6. The wing had a design lift coefficient of 0.08, a leading-edge sweep angle of 70°, and an aspect ratio of 2.24. Tests of each of three wing-body-nacelle configurations were conducted through an angle-of-attack range from -4° to 6° for nacelle alinement angles from -4° to 6°. Sidewash angles at the nacelle locations were measured through the angle-of-attack range and are compared with theoretical estimates.

The minimum incremental drag due to a nacelle or a combination of nacelles occurs at or near a nacelle alinement angle one-half the sidewash angle or one-half the average sidewash angle, respectively. Addition of the nacelles has little or no effect on the lift-curve slope, the slope of the curve of the pitching moment with respect to lift, or the drag due to lift.

INTRODUCTION

Beneficial interference effects caused by engine nacelles on wing-body aerodynamic characteristics have been observed on several representative supersonic-transport configurations. Data presented in reference 1 for two complex airplane configurations which employ highly swept twisted-and-cambered arrow-wing planforms show some very favorable component-interference effects at lifting conditions. These beneficial effects exist for both flat and twisted-and-cambered wings regardless of wing design lift coefficient, but they are not fully understood and no attempt has been made to optimize them. The results of reference 2 indicate that when wing-mounted nacelles or stores are oriented so as to minimize their drag contribution at some lifting condition, they can produce rather large increments in drag at negative lift conditions because of nacelle misalinement with the local wing sidewash. At some positive value of lift the body becomes alined with the local flow, and at slightly higher values a thrust component of the body side force may be generated.

The purpose of the present investigation is to determine how sensitive the interference effects of engine placement are to nacelle alinement with respect to the wing sidewash field. Aerodynamic characteristics were obtained for three twisted-and-cambered wing-body-nacelle configurations: one with a nacelle at 27 percent of the wing semispan; one with a nacelle at 50 percent of the wing semispan; and one with two nacelles, one at 27 percent and the other at 50 percent of the wing semispan. Tests of each wing-body-nacelle configuration were conducted through an angle-of-attack range from -4° to 6° for nacelle alinement angles from -4° to 6° at a Reynolds number based on the wing mean aerodynamic chord of 4.05×10^{6}.

SYMBOLS

b	wing span
c	local wing chord
$\bar{c}$	wing mean aerodynamic chord
C_D	drag coefficient, $\frac{\text{Drag}}{qS}$
C_L	lift coefficient, $\frac{\text{Lift}}{qS}$
C_{L_α}	wing lift-curve slope, $\frac{\partial C_L}{\partial \alpha}$
$\left(C_{L_\alpha}\right)_n$	nacelle lift-curve slope
C_m	pitching-moment coefficient measured about $\bar{c}/4$, $\frac{\text{Pitching moment}}{qS\bar{c}}$
$C_{m_{C_L}}$	slope of curve of pitching moment with respect to lift, $\frac{\partial C_m}{\partial C_L}$
l	overall length of wing measured in streamwise direction
q	free-stream dynamic pressure
r	radius of body or nacelle
S	semispan-wing area
x,y,z	Cartesian coordinate system in which X-axis is the intersection of the wing horizontal reference plane and the wing-body vertical plane of symmetry, origin at body nose, X-axis streamwise
x'	distance from wing leading edge measured in the x-direction

x''	distance from nacelle apex measured in the x-direction
α	angle of attack
ν	nacelle alinement angle, positive when rear of nacelle is outboard
σ	sidewash angle
ΔC_D	increment in drag coefficient due to nacelle
ΔC_Y	force coefficient perpendicular to nacelle in xy-plane

MODEL AND INSTRUMENTATION

A drawing of the test wing-body configuration showing nacelle location is presented in figure 1. Nacelle ordinates are given in table I. The nacelles were mounted on pylons below the wing lower surface. The distance between the wing surface and the nacelle was equal to the maximum radius of the nacelle when the nacelle was alined with the free stream. Nacelle orientation was varied by rotation of the pylon-mounted nacelles about the nacelle apex; positive orientation angles were those with the rear of the nacelle outboard. The apex of the nacelle at 27 percent of the wing semispan was at 60 percent of the local wing chord; the apex of the nacelle at 50 percent of the wing semispan was at 45 percent of the local wing chord.

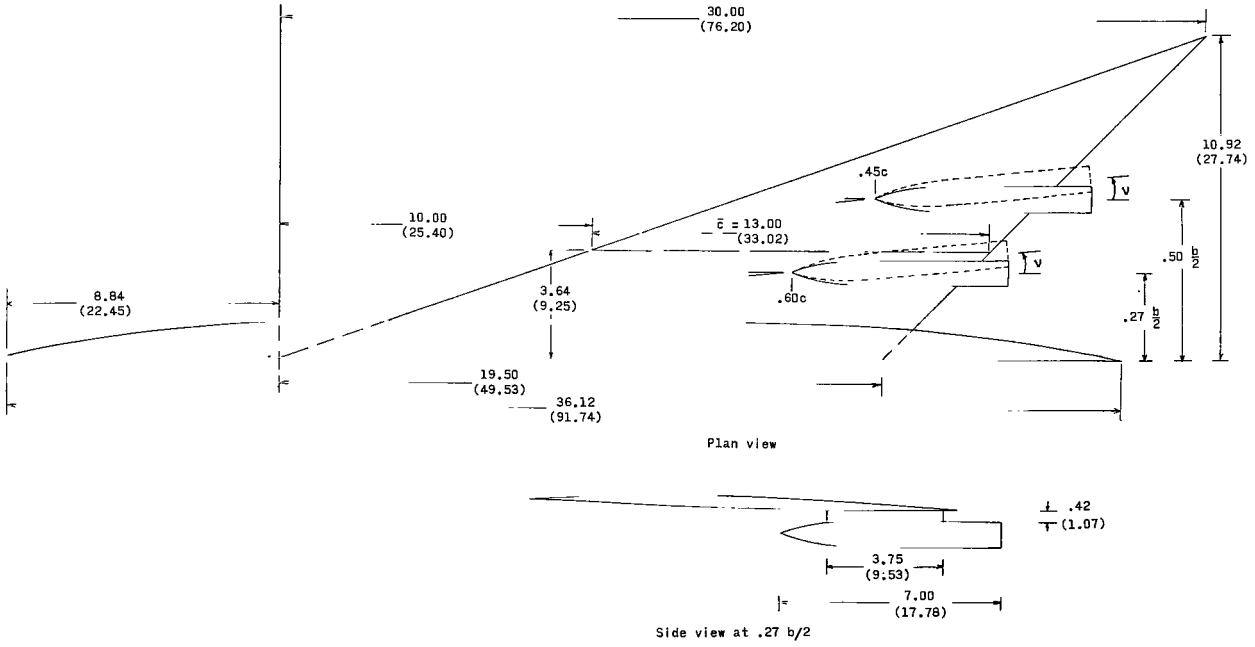

Figure 1.- Sketch of model. All dimensions are in inches. (Parenthetical dimensions are in centimeters.)

TABLE I.- NACELLE ORDINATES

x"		r	
in.	cm	in.	cm
0	0	0	0
.20	.51	.100	.254
.40	1.02	.165	.419
.60	1.52	.215	.546
.80	2.03	.250	.635
1.20	3.05	.312	.792
1.60	4.06	.350	.889
2.00	5.08	.377	.958
2.50	6.35	.397	1.008
3.00	7.62	.408	1.036
4.00	10.16	.420	1.067
↓	↓	↓	↓
7.00	17.78	.420	1.067

Body ordinates are given in table II. The body has a fineness ratio of 14.5 and is geometrically identical to the uncambered body of reference 3. The center line of the body is alined with the wing root chord.

TABLE II.- BODY ORDINATES

x		r	
in.	cm	in.	cm
0	0	0	0
1.04	2.64	.240	.610
2.08	5.28	.455	1.156
3.12	7.92	.642	1.631
4.16	10.57	.794	2.017
5.20	13.21	.927	2.355
6.24	15.85	1.040	2.642
7.28	18.49	1.125	2.858
8.32	21.13	1.185	3.010
9.36	23.77	1.223	3.106
10.40	26.42	1.240	3.150
↓	↓	↓	↓
24.24	61.57	1.240	3.150

x		r	
in.	cm	in.	cm
25.23	64.08	1.228	3.119
26.22	66.60	1.200	3.048
27.21	69.11	1.159	2.944
28.20	71.63	1.098	2.789
29.19	74.14	1.022	2.596
30.18	76.66	.925	2.350
31.17	79.17	.815	2.070
32.16	81.69	.688	1.748
33.15	84.20	.544	1.382
34.14	86.72	.382	.970
35.13	89.23	.200	.508
36.12	91.74	0	0

The highly swept twisted-and-cambered wing has a design lift coefficient of 0.08 and is geometrically identical to wing 2 of reference 4. The wing has a 70° swept leading edge and an aspect ratio of 2.24. The thickness distribution of the wing was formed by a 3-percent-thick circular-arc airfoil section in the streamwise direction. This thickness was added symmetrically to the mean-camber surface ordinates. Nondimensional mean-camber surface ordinates are given in table III.

TABLE III.- WING-CAMBER SURFACE ORDINATES $\frac{z}{lC_{L,design}}$

$\frac{x'}{c}$	$\frac{z}{lC_{L,design}}$ for $y/\frac{b}{2}$ of -										
	0	0.10	0.20	0.30	0.40	0.50	0.60	0.70	0.80	0.90	1.00
0	0.4000	0.1566	0.0550	0.0170	0.0226	0.0280	0.0326	0.0380	0.0433	0.0480	0.0533
.025	.3866	.1593	.0580	.0223	.0266	.0320	.0366	.0420	.0476	.0496	
.050	.3700	.1593	.0620	.0256	.0300	.0350	.0400	.0446	.0486	.0506	
.100	.3366	.1533	.0620	.0290	.0353	.0400	.0453	.0500	.0533	.0533	
.200	.2733	.1233	.0480	.0230	.0370	.0456	.0520	.0566	.0590	.0573	
.300	.2020	.0870	.0270	.0110	.0320	.0450	.0540	.0600	.0640	.0610	
.400	.1300	.0430	0	-.0040	.0250	.0400	.0520	.0620	.0666	.0646	
.500	.0580	-.0040	-.0280	-.0220	.0146	.0333	.0500	.0616	.0680	.0670	
.600	-.0170	-.0533	-.0590	-.0433	.0020	.0250	.0460	.0600	.0686	.0690	
.700	-.0980	-.1000	-.0906	-.0650	-.0103	.0150	.0373	.0570	.0686	.0710	
.800	-.1800	-.1433	-.1240	-.0883	-.0250	.0040	.0316	.0540	.0680	.0726	
.900	-.2640	-.1876	-.1560	-.1133	-.0430	-.0080	.0260	.0500	.0666	.0736	
1.000	-.3466	-.2296	-.1850	-.1350	-.0600	-.0213	.0180	.0453	.0653	.0746	

The body was attached to the half-span steel wing, which in turn was mounted on a four-component strain-gage balance housed within a horizontal boundary-layer-bypass plate. The plate was supported by the permanent sting mounting system of the Langley 4- by 4-foot supersonic pressure tunnel. During the tests, the entire plate-balance-model arrangement moved as a single unit through an angle-of-attack range. A very small gap between the plate and the bottom surface of the wing-body configuration was provided to prevent fouling between the plate and the model during the tests.

Sidewash angles were measured at the location of each nacelle apex by means of conical probes. Each probe had a total head orifice and four static-pressure orifices located at 90° intervals around the probe. Probe pressures were measured by individual pressure gages and the outputs from these gages were digitized and recorded on punch cards.

The base pressure of the nacelles was measured by means of a static-pressure orifice located within the nacelle-base cavity.

TESTS AND CORRECTIONS

The tests were conducted in the Langley 4- by 4-foot supersonic pressure tunnel at a Mach number of 2.03 and a Reynolds number based on the wing mean aerodynamic chord of 4.05×10^6. In order to insure a turbulent boundary layer, 0.125-inch-wide (0.318 cm) strips of No. 60 carborundum grains in a lacquer binder were used. Strips were placed 0.25 inch (0.635 cm) behind the leading edge on both surfaces of the wing, 1.25 inches (3.175 cm) behind the nose of the body, 0.25 inch (0.635 cm) behind the pylon leading edge, and 0.50 inch (1.270 cm) behind the nacelle apex.

The angle-of-attack range for each of three wing-body-nacelle configurations was from -4° to 6° for nacelle alinement angles of -4°, 0°, 2°, 4°, and 6°. The angle of attack was measured optically with the use of a prism recessed in the body of the model.

The three wing-body-nacelle configurations were: one with a nacelle at 27 percent of the wing semispan; one with a nacelle at 50 percent of the wing semispan; and one with two nacelles, one at 27 percent and the other at 50 percent of the wing semispan.

The sidewash angles at the two spanwise nacelle locations were measured through the angle-of-attack range used for the force tests.

The drag force was adjusted so that the base pressure of the nacelles would be equal to free-stream static pressure.

RESULTS AND DISCUSSION

Addition of the nacelles to the wing of the present investigation has little or no effect on C_{L_α}, $C_{m_{C_L}}$, or the drag due to lift. However, C_L increases and C_m for $C_L = 0$ decreases when the nacelles are added (fig. 2). Changing nacelle orientation has only a small effect on C_L and C_m at the positive nacelle alinement angles for the configurations with only one nacelle. For the configuration with two nacelles, the effect of changing nacelle orientation is somewhat larger. (See fig. 3.)

The increment in drag coefficient due to the nacelles ΔC_D is plotted in figure 4 as a function of nacelle orientation angle ν for three representative lift coefficients: $C_L = 0$, the design lift coefficient 0.08; and the lift coefficient for maximum lift-drag ratio 0.16. These data show that the minimum ΔC_D occurs somewhere between $\nu = 0^\circ$ and $\nu = 2^\circ$.

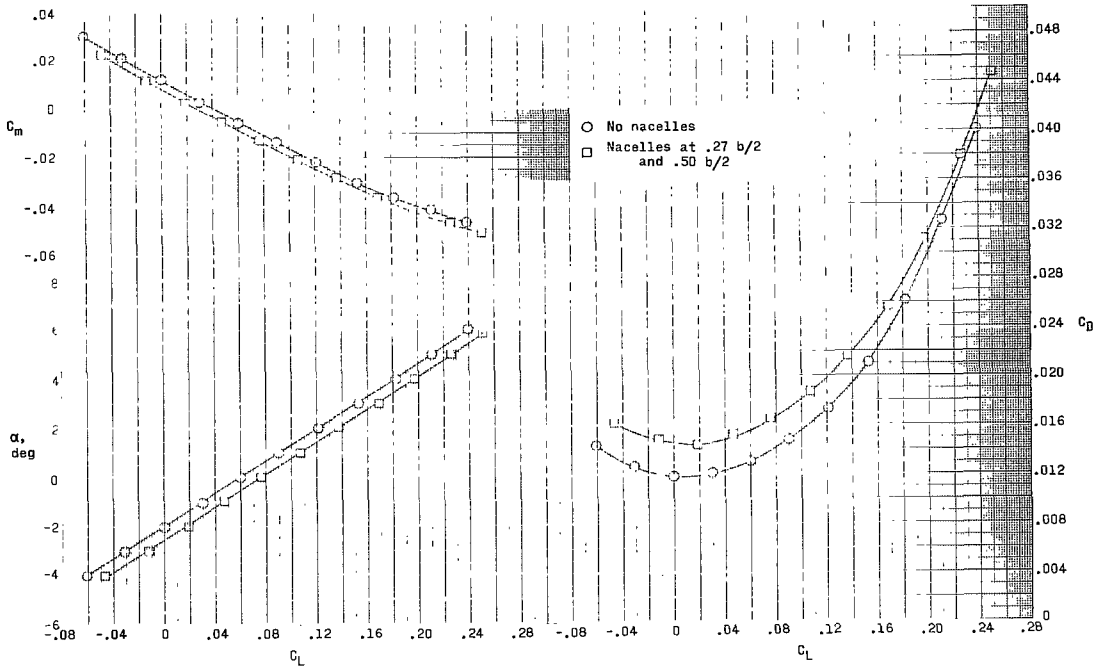

Figure 2.- Effect of nacelles on aerodynamic characteristics in pitch.

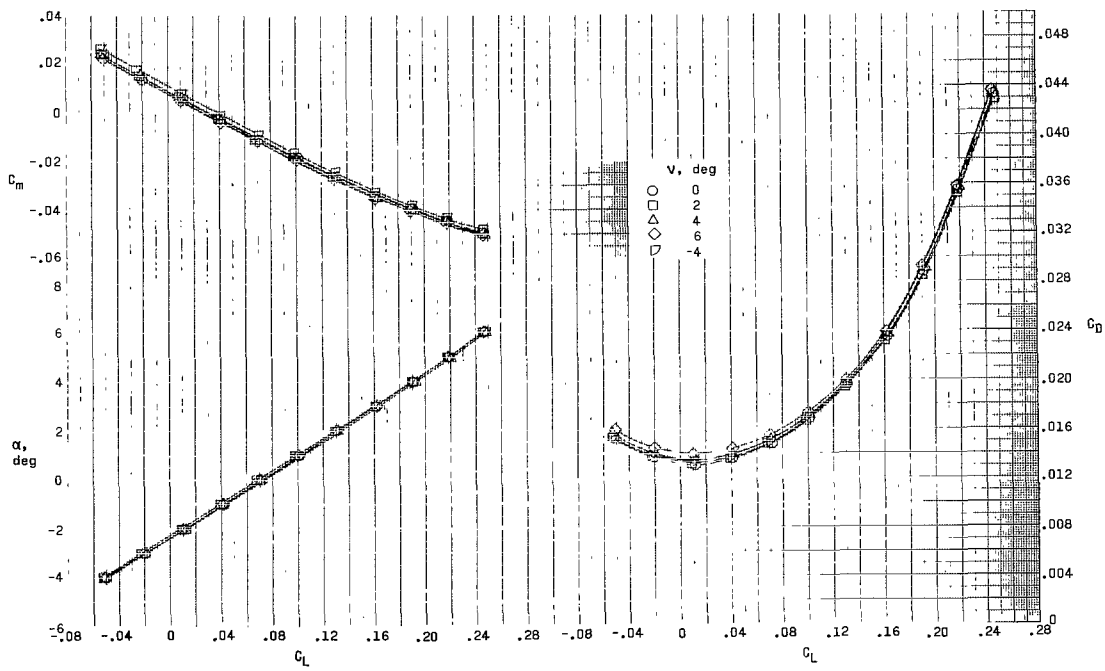

(a) Nacelle at 27 percent of wing semispan.

Figure 3.- Aerodynamic characteristics in pitch of wing-body-nacelle configurations.

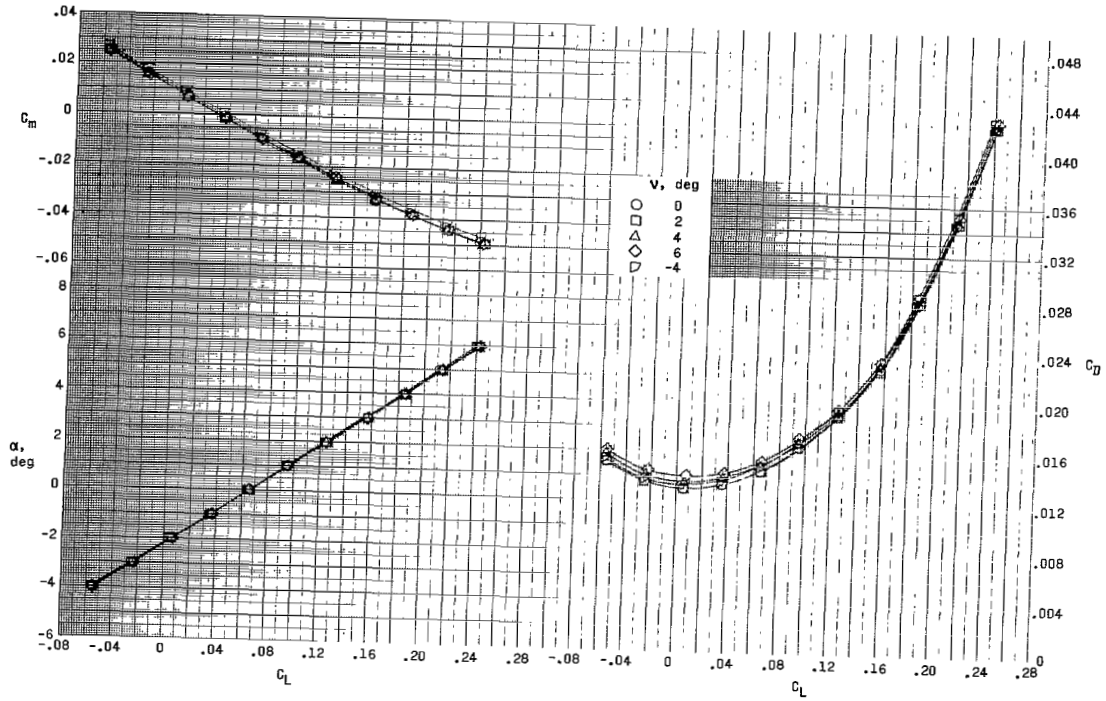

(b) Nacelle at 50 percent of wing semispan.

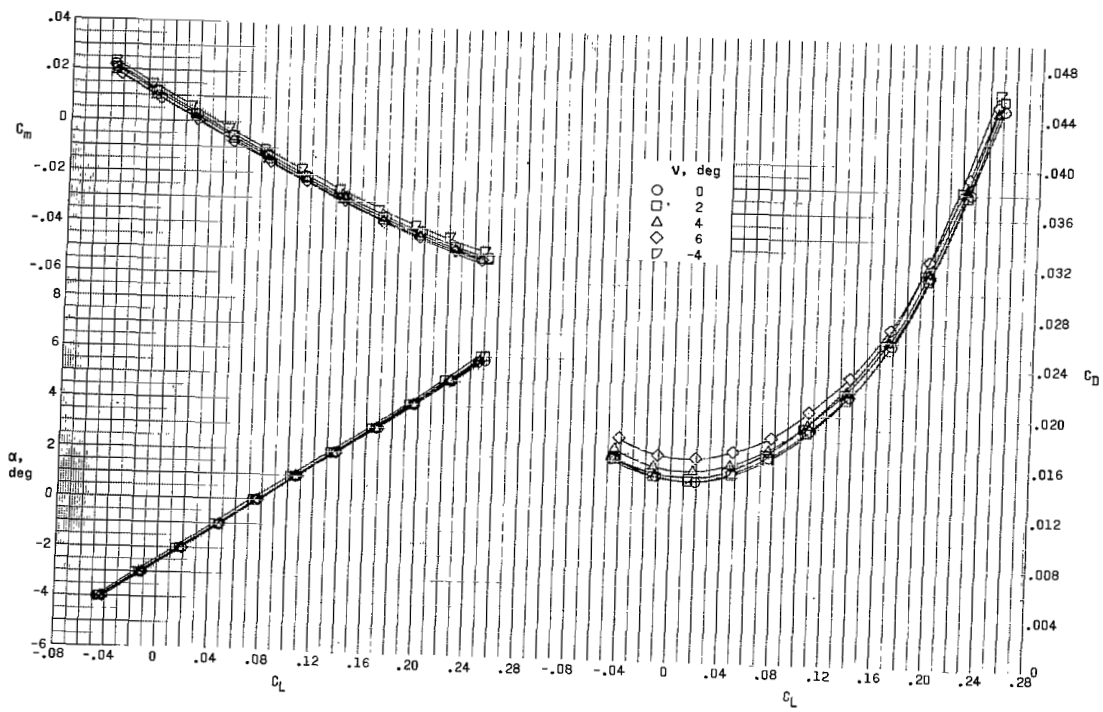

(c) Nacelles at 27 and 50 percent of wing semispan.

Figure 3.- Concluded.

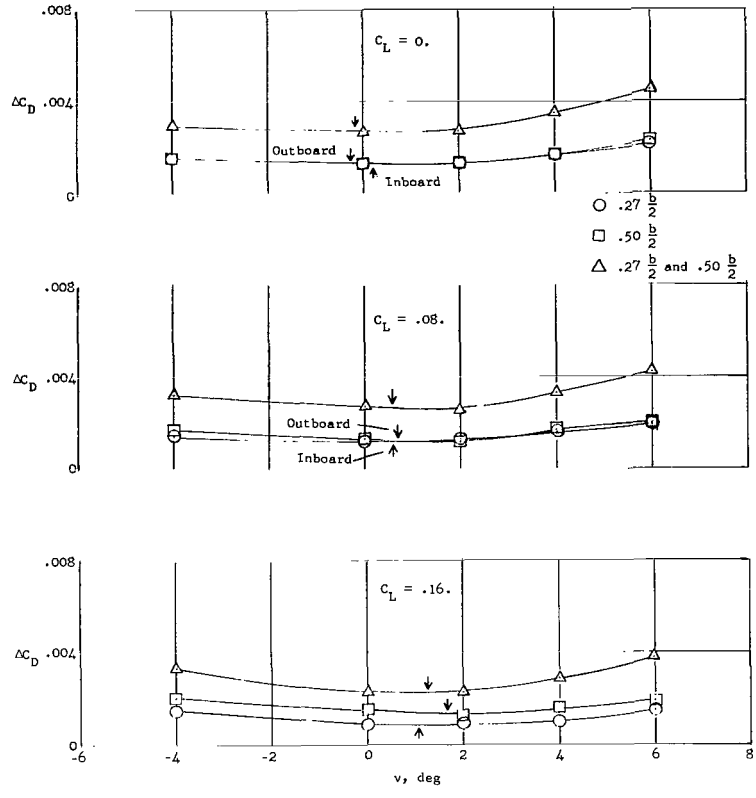

Figure 4.- Variation of incremental drag with nacelle orientation. Arrows indicate value of $\sigma/2$.

In order to analyze the effect of nacelle orientation further, a force perpendicular to the nacelle ΔC_Y in the xy-plane is assumed. (See sketch.) The nacelle is inclined at an angle ν with the free stream. The streamwise component ΔC_D of this normal force is negative and corresponds to a thrust. A nacelle orientation angle which will maximize this component and thereby minimize drag is desired.

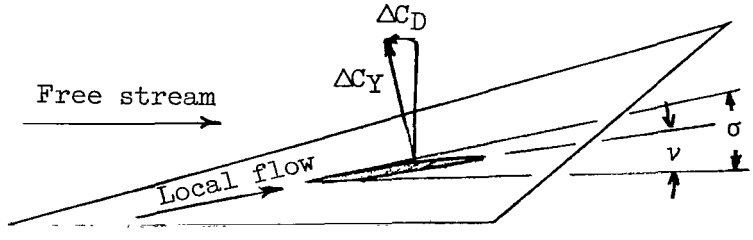

The component ΔC_D is $\Delta C_Y \sin \nu$, or for small values of ν, $\Delta C_D \approx \Delta C_Y \nu$. The force ΔC_Y may also be expressed in terms of the nacelle lift-curve slope $(C_{L_\alpha})_n$ and the alinement of the nacelle with respect to the sidewash field:

$$\Delta C_Y = \left(C_{L_\alpha}\right)_n(\nu - \sigma)$$

where σ is the sidewash angle. Combining the expressions for ΔC_D and ΔC_Y results in the following equations:

$$\Delta C_D = \left(C_{L_\alpha}\right)_n(\nu - \sigma)\nu$$

$$\Delta C_D = \left(C_{L_\alpha}\right)_n(\nu^2 - \nu\sigma)$$

Differentiating with respect to ν yields

$$\frac{\partial \Delta C_D}{\partial \nu} = \left(C_{L_\alpha}\right)_n(2\nu - \sigma)$$

and setting $\frac{\partial \Delta C_D}{\partial \nu} = 0$ shows that a maximum value of negative ΔC_D (minimum drag) exists when $\nu = \sigma/2$. Thus, these results indicate that the drag increment due to the addition of a nacelle is minimized when the nacelle is installed at an angle equal to half the sidewash angle. However, this analysis gives only an approximation of the optimum angle, inasmuch as the forces imposed on the wing surface by the nacelle are neglected.

Measured sidewash angles for the lift coefficients presented in figure 4 are given in the following table:

Nacelle location, percent of semispan	σ, deg, for -		
	$C_L = 0$ (a)	$C_L = 0.08$ (a)	$C_L = 0.16$ (a)
27	0.4	1.2	2.1
50	-.5	1.4	3.3
27 and 50	[b]-.3	[b]1.1	[b]2.5

[a] C_L is measured value at $\nu = 0^\circ$ for the nacelle configuration in question.

[b] Average of the values of σ for nacelles at 27 percent and 50 percent of wing semispan for C_L at $\nu = 0^\circ$ for configuration with both nacelles.

Comparison of the values of $\sigma/2$ as determined from the preceding table (shown as arrows in fig. 4) with the values of ν for minimum ΔC_D (0° to 2°) indicates very good agreement. Thus it appears that the minimum incremental drag due to a nacelle or a combination of nacelles occurs at or near an alinement angle of one-half the sidewash angle or one-half the average sidewash angle, respectively.

A comparison of the theoretical estimates of the sidewash angle with experimental values can be seen in figure 5. The theoretical sidewash angles were determined from the chordwise and spanwise slopes of the velocity potential, which was obtained from existing pressure distributions calculated by the method of reference 5 and unpublished computer programs. The effects of lift, camber, and thickness were accounted for in the calculations. For the wing of the present investigation, the measured sidewash angles are somewhat less than the theoretical values at positive angles of attack. Some of this difference may be due to the fact that surface pressures were used for the theoretical calculations, whereas the experimental angles were measured below the wing surface at a distance equal to the maximum nacelle radius.

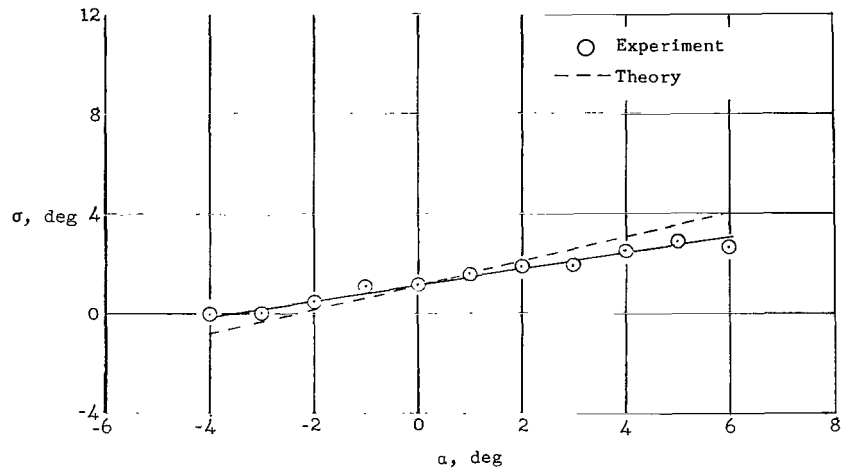

(a) Nacelle at 27 percent of wing semispan.

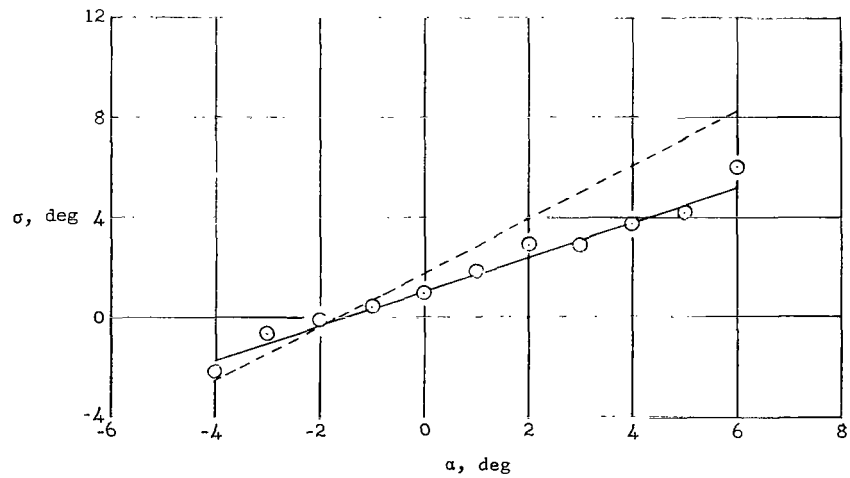

(b) Nacelle at 50 percent of wing semispan.

Figure 5.- Sidewash angles as a function of wing angle of attack.

CONCLUSIONS

The results of an investigation conducted in the Langley 4- by 4-foot supersonic pressure tunnel at a Mach number of 2.03 to determine the effect of nacelle alinement on the aerodynamic characteristics of a highly swept twisted-and-cambered arrow-wing-body-nacelle configuration indicate the following conclusions:

1. The minimum incremental drag due to a nacelle or a combination of nacelles occurs at or near a nacelle alinement angle of one-half the sidewash angle or one-half the average sidewash angle, respectively.

2. Addition of the nacelles has little or no effect on the lift-curve slope, the slope of the curve of the pitching moment with respect to lift or the drag due to lift.

Langley Research Center,
National Aeronautics and Space Administration,
Langley Station, Hampton, Va., December 2, 1965.

REFERENCES

1. McLean, F. Edward; and Fuller, Dennis E.: Supersonic Aerodynamic Characteristics of Some Simplified and Complex Aircraft Configurations Which Employ Highly Swept Twisted-and-Cambered Arrow-Wing Planforms. Vehicle Design and Propulsion. American Inst. Aeron. and Astronautics, Nov. 1963, pp. 98-103.

2. Robins, A. Warner; Morris, Odell A.; and Harris, Roy V., Jr.: Recent Research Results in the Aerodynamics of Supersonic Vehicles. Paper No. 65-717, Am. Inst. Aeron. Astronaut., Nov. 1965.

3. Carlson, Harry W.: Longitudinal Aerodynamic Characteristics at Mach Number 2.02 of a Series of Wing-Body Configurations Employing a Cambered and Twisted Arrow Wing. NASA TM X-838, 1963.

4. Carlson, Harry W.: Aerodynamic Characteristics at Mach Number 2.05 of a Series of Highly Swept Arrow Wings Employing Various Degrees of Twist and Camber. NASA TM X-332, 1960.

5. Middleton, Wilbur D.; and Carlson, Harry W.: A Numerical Method for Calculating the Flat-Plate Pressure Distributions on Supersonic Wings of Arbitrary Planform. NASA TN D-2570, 1965.

"The aeronautical and space activities of the United States shall be conducted so as to contribute . . . to the expansion of human knowledge of phenomena in the atmosphere and space. The Administration shall provide for the widest practicable and appropriate dissemination of information concerning its activities and the results thereof."

—NATIONAL AERONAUTICS AND SPACE ACT OF 1958

NASA SCIENTIFIC AND TECHNICAL PUBLICATIONS

TECHNICAL REPORTS: Scientific and technical information considered important, complete, and a lasting contribution to existing knowledge.

TECHNICAL NOTES: Information less broad in scope but nevertheless of importance as a contribution to existing knowledge.

TECHNICAL MEMORANDUMS: Information receiving limited distribution because of preliminary data, security classification, or other reasons.

CONTRACTOR REPORTS: Technical information generated in connection with a NASA contract or grant and released under NASA auspices.

TECHNICAL TRANSLATIONS: Information published in a foreign language considered to merit NASA distribution in English.

TECHNICAL REPRINTS: Information derived from NASA activities and initially published in the form of journal articles.

SPECIAL PUBLICATIONS: Information derived from or of value to NASA activities but not necessarily reporting the results of individual NASA-programmed scientific efforts. Publications include conference proceedings, monographs, data compilations, handbooks, sourcebooks, and special bibliographies.

Details on the availability of these publications may be obtained from:

SCIENTIFIC AND TECHNICAL INFORMATION DIVISION

NATIONAL AERONAUTICS AND SPACE ADMINISTRATION

Washington, D.C. 20546